Time-Integrated Pointers for Enabling the Analysis of Detailed Reaction Mechanisms

Ioannis P. Androulakis and Jeffrey M. Grenda
Corporate Strategic Research, ExxonMobil Research and Engineering, Annandale, NJ 08801

Joseph W. Bozzelli
Dept. of Chemistry, New Jersey Institute of Technology, Newark, NJ 07102

DOI 10.1002/aic.10263
Published online in Wiley InterScience (www.interscience.wiley.com).

A procedure for deriving time-integrated pointers to capture element transformations during numerical integration runs, on complex chemical mechanisms, is introduced. The principal advantage is that the resulting temporally integrated pointers allow derivation of importance criteria; and these weight the contribution of all species and reactions during the reaction interval. This approach quantifies the sources and sinks of reactions active over a period of time in terms of element flux. It provides identification of key reaction pathways and the derivation of a reduced skeletal representation at minimum computational cost, in the elementary mechanism analysis. We extend the analysis to more complex systems, such as burner-stabilized flames, that are governed by both reaction and diffusion. Here, we illustrate how some reaction pathways are altered in the presence of diffusion. Finally a new coupling of mechanism generation and mechanism reduction, which significantly reduces the computational burden associated with automated kinetic mechanism generation, is presented. The concepts are demonstrated with examples involving high- and low-temperature oxidation of hydrocarbons. © 2004 American Institute of Chemical Engineers *AIChE J,* 50: 2956–2970, 2004

Introduction

The demand for detailed fundamental kinetic mechanisms continues to be driven by the desire to develop methods for making accurate predictions and optimizing processes involving complex chemical reacting systems, such as hydrocarbon or waste combustion and atmospheric chemistry. Use of accurate mechanisms for fundamental chemical understanding to achieve controls or optimum conversion is important for such a process to achieve improved efficiency or meet projected environmental regulations.

Numerous detailed kinetic mechanisms have been manually constructed for a wide range of combustion and chemical process applications (Curran et al., 1998a,b; Dean, 1990; Mims et al., 1994; Westbrook, 2002). Most models are constructed based on extensive compilations of elementary chemical reactions, using kinetic parameters derived from a combination of experimental measurements, model estimates from computational chemistry, and generic estimation of thermodynamic properties. Significant activity has been directed at understanding the fundamental processes associated with hydrocarbon oxidation and internal combustion engine efficiency by using models to optimize the combined engine–fuel system (Callahan et al., 1996; Kimura et al., 2001; Westbrook et al., 2001). Several models have been presented, for example, that extend prototype fuel feeds into the octane range, where these are related to ongoing low-temperature combustion improvements in automotive applications.

There are also positive computational advances enabling automated kinetic mechanism generation (Broadbelt et al.,

Correspondence concerning this article should be addressed to I. P. Androulakis at Chemical and Biochemical Engineering Dept., Rutgers-The State University of New Jersey, Piscataway, NJ 08854; E-mail: yannis@rci.rutgers.edu.

1994; Chevalier et al., 1992; Grenda et al.; 2001, 2002; Susnow et al., 1997; Warth et al., 2000). These codes enable the generation of such mechanisms; but the mechanisms are usually so large, that are they difficult to implement directly. The generated models provide significant kinetic insight and modeling capabilities, but also have major difficulties in application because of the enormous number of species and reactions that are created. Models often include up to a thousand or more species and several thousand chemical reactions (Curran et al., 1998). As the emphasis continues to be placed on kinetic models that retain a wide operating range of applicability, the reaction models will continue to increase in size.

The problems associated with mechanism size are twofold. First, large mechanisms make the identification and extraction of kinetically important species and reactions difficult. As the chemical reaction process unfolds, many processes exhibit a series of selected kinetic stages where pathway importance increases and later diminishes. The kinetic importance of species and/or reactions is time dependent and the temporal contributions are not known beforehand. This makes manual identification by traditional instantaneous sensitivity analyses difficult. The second difficulty with large mechanisms is the inability to couple such kinetic models with computational fluid dynamics (CFD) simulations, which prevents their application to practical industrial systems where significant mixing or other nonhomogeneous conditions may be dominant.

A number of model reduction approaches have been proposed in an attempt to identify reduced subset representations or by developing alternative representations of the detailed mechanism that can be used with CFD calculations. A recent review can be found in Tomlin et al. (1997).

The approach in this study follows the transformation of elements (such as hydrogen, carbon, oxygen, and so on, from reactants to intermediates to products) over time intervals. We demonstrate how temporal dependencies can be removed, by appropriate integration of flux pointers, to derive time-independent skeletal pathways. These pointers allow the derivation of importance criteria that weight the contribution of reacting species. The overall analysis provides key improvements to the evaluation of the chemical kinetics, species reduction, and use of automated mechanism generation.

This study includes:

(1) Obtainment and use of time-integrated quantities, unlike previous analyses that use only temporal metrics.

(2) Demonstration of a framework applicable to systems involving both chemical reaction and diffusion, unlike previous approaches that decouple transport and chemistry to analyze the kinetic mechanism.

(3) A novel automated integration of mechanism generation and mechanism reduction, to address problems associated with generation of very large mechanisms, which limit the applicability of current automated mechanism generation schemes.

We describe the computational methodology and subsequently use several examples illustrating the approach. The examples cover a wide range of reacting conditions including high- and low-temperature oxidation, pyrolysis, and flame-stabilized calculations.

Time-Integrated Analysis of Detailed Kinetic Mechanisms

Instantaneous element flux analysis

The concept of *element flux analysis*, introduced by Revel et al. (1994), allows one to develop time-dependent flux diagrams that identify key reaction pathways with minimal effort. The main idea is to study principal reaction pathways along the reaction process coordinate. The atomic fluxes for each atom (C, H, O, N, Cl, S) at different reaction times are calculated, based on reaction rates, and the major sources and sinks for each element are identified. According to Revel et al. (1994), the instantaneous chemical flux of atom A from species j to species k through reaction i is defined as

$$\dot{A}_{ijk} = q_i \frac{n_{A,j} n_{A,k}}{N_{A,i}} \tag{1}$$

where q_i is the net production rate of reaction i (mol s^{-1}), $n_{A,j}$ is the number of atoms A in species j, $n_{A,k}$ is the number of atoms A in species k, and $N_{A,i}$ is the total number of atoms of element A in reaction i. This definition allows the atomic fluxes through a given reaction to be distributed between the different species of the reaction. To illustrate the definition let us consider the simple reaction

$$CH_4 \rightarrow CH_3 + H \tag{2}$$

If we consider the flow of H mass, according to the definition given by Eq. 1, then we have

$$A_{CH_4 \rightarrow CH_3} = q \frac{4 \times 3}{8} = 3\frac{q}{2} \qquad A_{CH_4 \rightarrow H} = q \frac{4 \times 1}{8} = \frac{q}{2} \tag{3}$$

where q stands for the net rate of the reaction. Here, three times more H ends in the methyl radical than atomic H. For any given atom (A), we can then consider the transformations that occur from species to species, by all reactions in the network. The total transfer of element mass for any pair of species accounting for all reactions (i) that these species participate as reactants/products, as a function of time t, can then be defined as

$$\bar{A}_{\mathrm{FROM,TO}}(t) = \sum_{i=1}^{N_R} A_{i,\mathrm{FROM,TO}}(t) \tag{4}$$

The computational model used in the calculation of the quantities in Eq. 4 is a premixed plug-flow reactor model. The governing equations are

$$\frac{dy_s}{dz} = \sum_{r=1}^{N_R} \alpha_{rs} R_r \qquad \frac{dT}{dz} = \sum_{s=1}^{N_S} H_s^g \frac{dy_s}{dz}$$

$$R_r = K_r^F e^{-E_r/RT} \prod_{s=1}^{N_S} [X_s]^{\alpha'_{rs}} - K_r^R e^{-E_r/RT} \prod_{s=1}^{N_S} [X_s]^{\alpha''_{rs}}$$

$$y_s(0) = y_s^0 \qquad T(0) = T^0 \tag{5}$$

Equation 5 defines the standard heat and material balance. Species mass fractions are denoted by y; molar concentrations are denoted by X; the stoichiometric coefficient of species "s" in reaction "r" is denoted by α; H is the specific enthalpy of species "s"; K denotes rate constants; and E is the activation energy. The superscript 0 denotes initial conditions. The thermophysical properties and reaction rate definitions are handled using CHEMKIN (Kee et al., 1996).

Most standard stiff integrators can be used for the integration of the above systems on nonlinear ordinary differential equations. A plug-flow reactor (PFR) model has been selected, although any other reactor model can be used. It will be shown below how this analysis can be extended, in a postprocessing mode, to more complex reaction–diffusion models.

A novel time-integrated element flux analysis

The fluxes defined in Eq. 4 are functions of time. Therefore, one repeats the analysis at preselected time instances during the reaction process. This is equivalent to taking snapshots during the reaction and trying to identify, in time, active sources and sinks. These flowcharts can then be used to identify reaction pathways as they develop over time. The approach as described makes it cumbersome to derive *global information*. The fluxes have to be constructed at selected points in time. However, the time points at which these computations are performed are not always evident.

Here we introduce the concept of a *time-integrated flux indicator*. The main idea is to derive (over time) an indicator for a *source–sink* combination based on integration of the quantity defined in Eq. 4. The quantity will be subsequently normalized as a means of representing the results. Therefore, we define the quantity

$$\hat{A}_{\mathrm{FROM,TO}} = \frac{\int_{t=0}^{\tau} \bar{\dot{A}}_{\mathrm{FROM,TO}}(t)dt}{\Sigma_{\mathrm{FROM}'}\,\Sigma_{\mathrm{TO}'}\int_{t=0}^{\tau} \bar{\dot{A}}_{\mathrm{FROM}',\mathrm{TO}'}(t)dt} \tag{6a}$$

The integrals in Eq. 6a are estimated numerically by accounting for all the time instances as the integrator is generating them. In this way, the entire reaction trajectory is taken into account, and there is no need to *a priori* select the location of the snapshots. The quantity defined in Eq. 6a allows one to assign a unique, overall number to each *source–sink* pair, which is representative of the entire reaction period. The normalization defined in Eq. 6a ensures that pathways activated at different points in time receive appropriate weighting.

Similarly, a different type of normalization can be defined as

$$\hat{A}_{\mathrm{FROM,TO}} = \frac{\int_{t=0}^{\tau} \bar{\dot{A}}_{\mathrm{FROM,TO}}(t)dt}{\max\int_{t=0}^{\tau} \bar{\dot{A}}_{\mathrm{FROM,TO}}(t)dt} \tag{6b}$$

This normalization is particularly helpful so as to report all possible transformations relative to the input channel (that is, fuel decomposition in combustion). In a subsequent section we will demonstrate its usefulness.

Time-integrated element flux analysis allows one to characterize the main transformations that take place during the reaction period. The analysis reveals key pathways in terms of source–sink relationships. However, this analysis does not reveal any information related to the way (specific reaction path) these transformations take place. The purpose of the time-integrated element flux analysis is to establish "global" insight into the reaction pathways. It allows for a comprehensive and macroscopic view of the reactant transformation to intermediate(s) and finally to products. By removing the temporal dependency it makes it possible to establish these types of relations.

Once the skeletal mechanism has been derived, one can follow this analysis with more detailed rate or sensitivity analysis to determine the most significant reaction path contributors to specific transformations. Time-integrated analysis corroborates the interpretations derived from instantaneous rate and sensitivity analysis. The results that follow will establish several points: the time-integrated element flux analysis is a powerful method for identifying skeletal mechanisms with excellent predictive capabilities and it generates significant chemical insight into complex kinetic mechanisms.

Computer implementation

For completeness and possible application by the reader, we present a CHEMKIN-like pseudocode for estimating the quantities defining the element transfer from species FROM to species TO. The nomenclature used is the standard CHEMKIN nomenclature. The flux is estimated at every time step (IT). We loop over all reactions (NII) and identify all species participating in each reaction (K and K1) in each integration step. If such a pair, such as (CH_4, CH_3), contains the element of interest, such as C, denoted as (NCF(NELE,K).GT.0) whose flux we wish to monitor, we use the stoichiometric coefficients (ISTOIC and ISTOIC1) to determine whether the species have a reactant/product relationship (ISTOC*ISTOC1 .lt. 0). The net rate of reaction (QQ(I)) determines the "direction" of mass flux and properly assigns K and K1 the role of source/sink (source species: IFROM, sink species: ITO). The temporal pointer AJK(IFROM, ITO, IT) is created and stored. To avoid the creation of huge matrices in the IT dimension, the integration is performed in small batches. Thus only a small number (50) of time intervals is actually stored. The main memory requirement of the method, therefore, scales as Nspecies^2. Once the time-dependent quantities AJK(IFROM,ITO,IT) are integrated numerically over the reaction interval IT=0, . . . , Final_Time we obtain the time-integrated pointer, indicating the importance of the transformation (IFROM, ITO). An exempt from our Fortran implementation is provided that uses actual CHEMKIN nomenclature:

```
• ICWKR    : CHEMKIN work array containing all necessary information for describing the
  reactions and the associated thermodynamics
• NI       : number of reactions in the mechanism
• MXSP     : maximum species allowed per reaction
• ICNK     : memory location defined by CHEMKIN
• ISTOIC   : stoichiometirc coefficient
• NCF      : CHEMKIN function determining whether species "K" contains element "NELE"
• QQ       : array containing rate of reaction calculated internally via CHEMKIN
    DO I = 1, NII
      DO N = 1, MXSP-1
        K = ICKWRK(ICNK + (I-1)*MXSP + N - 1)
        IF (K .NE. 0 .AND. NCF(NELE,K) .GT. 0) THEN
          ISTOIC=ICKWRK(ICNU+(I-1)*MXSP+N-1)
          DO N1=N+1, MXSP
            K1=ICKWRK(ICNK + (I-1)*MXSP + N1 - 1)
            IF(K1 .NE. 0 .AND. NCF(NELE,K1) .GT. 0) THEN
              ISTOIC1=ICKWRK(ICNU+(I-1)*MXSP+N1-1)
              IF(K.NE.K1.AND.ISTOIC*ISTOIC1.LT.0) THEN
                IF(QQ(I)*ISTOIC .LT. 0.0) THEN
                  IFROM=K
                  ITO=K1
                  NAJ=ABS(ISTOIC) * NCF(NELE,IFROM)
                  NAK=ABS(ISTOIC1) * NCF(NELE,ITO)
                ELSE
                  IFROM=K1
                  ITO=K
                  NAJ=ABS(ISTOIC1)* NCF(NELE,IFROM)
                  NAK=ABS(ISTOIC) * NCF(NELE,ITO)
                ENDIF
                AJK(IFROM,ITO,IT)=AJK(IFROM,ITO,IT)
                  + ABS(QQ(I))*NAJ*NAK/(NAI(I))
              ENDIF
            ENDIF
          ENDDO
        ENDIF
      ENDDO
    ENDDO
```

Interpreting the Time-Integrated Pointers. To illustrate the process we consider a case simulating a PFR with a mixture of methane/oxygen = 0.05/0.95 (mol ratio) input at inlet $T = 1000$ K. The model is an adiabatic PFR. The kinetics is simplified because the mixture is highly combustible and the fuel is consumed in its entirety. Table 1 summarizes the analysis output for GRIMECH30. The first two columns represent the (IFROM, ITO) pairs of elements when considering C transfer. The third column is the integrated normalized pointer (that is, Eq. 6a), the fourth column is a running sum, and the fifth column is the flux pointer normalized relative to the input channel.

Inspection of the data illustrates that a number of interesting observations can be made. Simply by sorting the pairs in descending order, we identify the leading reactant [intermediate (i), intermediate (ii), and so forth] couples in the chemical transformations. The running sum indicates the transformations that contain the leading transitions. By setting a user-selected cutoff value we can determine which transitions describe the majority of the carbon fluxes. For example, if we set the cutoff at less than 90% carbon flux, we identify that the species CH4, CH3, CH3O, CH2O, HCO, CO, and CO2 are adequate for capturing the major element transformations. This user-defined cutoff is a critical parameter that will be used in later sections of this report to define skeletal mechanisms. The process of identifying the skeletal transformations is depicted in Figure 1. The carbon flux is material balanced once additional transformations involving "minor" species are included (species in boxes). The point of the simulation is to illustrate the type of generated information. It is not meant to imply that a skeletal methane oxidation mechanism should be composed of only seven species. However, for oxygen-rich con-

Table 1. Sample Interpretation of the Time-Integrated Element Flux Pointers*

IFROM	ITO	Time-Integrated Flux Pointer AJK(IFROM,ITO)	Running Sum	Flux Pointer Relative to Input Channel
CH4	CH3	16.8	16.8	100.0
CO	CO2	16.8	33.6	100.0
HCO	CO	14.8	48.4	88.1
CH2O	HCO	14.2	62.6	84.5
CH3O	CH2O	12.2	74.8	72.6
CH3	CH3O	12.1	86.9	72.0
CH3	CH2O	1.9	88.8	11.4
C2H5	C2H4	1.1	90.0	6.8
CH3	C2H6	1.1	91.1	6.7
C2H6	C2H5	1.1	92.2	6.6
CH3	CH2(S)	1.0	93.2	6.0
CH2(S)	CO	0.9	94.1	5.5
C2H4	C2H3	0.6	94.7	3.4
CH3	CO	0.5	95.2	3.0
CH2CHO	CH2CO	0.5	95.7	2.8
HCCO	CO	0.4	96.1	2.5
CH2CO	HCCO	0.4	96.5	2.4
C2H3	CH2CHO	0.4	96.8	2.1
CH3	HCO	0.2	97.1	1.4
CH2O	CH4	0.2	97.3	1.4
C2H4	CH2CHO	0.2	97.5	1.2
CH3OH	CH2OH	0.1	97.6	0.8
CH3	CH3OH	0.1	97.7	0.6
C2H4	HCO	0.1	97.8	0.6
C2H4	CH3	0.1	97.9	0.6
CH2OH	CH2O	0.1	98.0	0.6
C2H3	HCO	0.1	98.1	0.5
C2H3	CH2O	0.1	98.2	0.5
CH3OH	CH3O	0.1	98.3	0.5
CH2	CO2	0.1	98.4	0.4
CH3	CH2	0.1	98.4	0.4
CH2	CO	0.1	98.5	0.4
CH2(S)	CH2	0.1	98.6	0.4

*The 90% carbon flux cutoff identifies a minimal set of seven species.

ditions at elevated temperatures this appears to be an excellent approximation for the mechanism used.

Time-integrated element flux pointer calculation in reaction–diffusion systems

The above analysis assumes that the data required for the integration of the reaction pointers are generated on-line by the integration of a system similar to the one described by Eq. 5; however, the approach is nonspecific and can be used in a more general way. The approach has been applied in the analysis of reaction pathways as they develop in more complex environments such as flame calculations. In this case the estimation of the species profiles is done off-line, taking into account both reaction and diffusion, through the solution of appropriate boundary value problems. These profiles are then postprocessed to estimate the quantities required for the derivation of the time-integrated pointers. In a later section we discuss the effects relative to chemistry in a way that the leading pathways are altered. This is a fundamental novelty of our approach because, for the first time, we are able to account for the impact of diffusion on the evolution of the chemical pathways. Although we selected to study a flame-propagation problem, we are currently exploring more complex reaction–diffusion systems. In practice we repeat the process described earlier in the pseudocode. The rates of reaction are again calculated using CHEMKIN with the mass fractions from the SANDIA Flame code being used for estimating the net rate of reaction.

Analysis and Reduction of Detailed Kinetic Mechanisms

Construction of time-integrated element flux diagrams

Stoichiometric High-Temperature Methane Oxidation. Time-integrated element flux diagrams for a stoichiometric mixture of methane/air at 1 atm with initial temperature of 1000 K during an adiabatic combustion were generated. Two independently developed mechanisms are analyzed:

(1) The GRIMECH3.0 with 53 species and 325 reactions

(2) A reaction mechanism developed by Mims et al. (1994), with 116 species and 457 reactions

This example is selected because methane oxidation pathways are fairly well understood with a consistent set of critical reaction steps identified. The results of the comparison are summarized in Figure 2. We observe that both mechanisms follow qualitatively very similar decomposition pathways. However, the relative magnitude of the individual paths (illustrated by different widths of the respective arrows) establishes the fundamental differences between the two schemes. That is, the Mims et al. (1994) mechanism has a higher propensity of preferentially converting methane to ethane, which is subsequently combusted, whereas the GRI 3.0 mechanism clearly favors the more direct fuel decomposition. Eventually, because

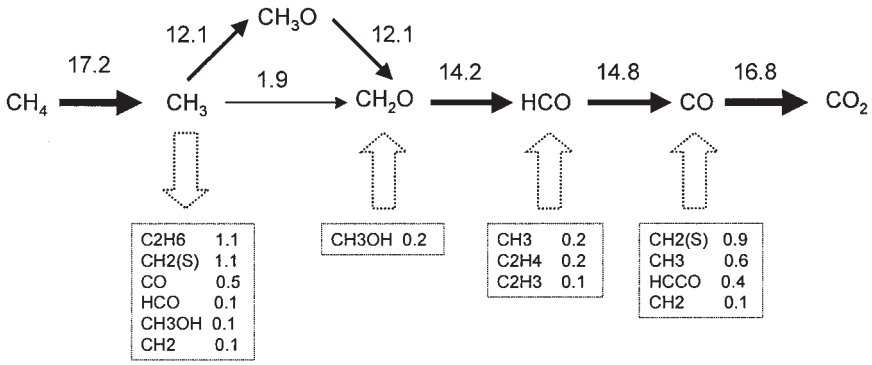

Figure 1. Time-integrated flux pathway analysis.

Adiabatic, PFR simulation, $T^0 = 1000$ K, methane:oxygen = 0.05:0.95, $P = 10$ atm. Based on the carbon flux analysis almost the entirety of the incoming carbon is recovered as CO_2 by this main pathway.

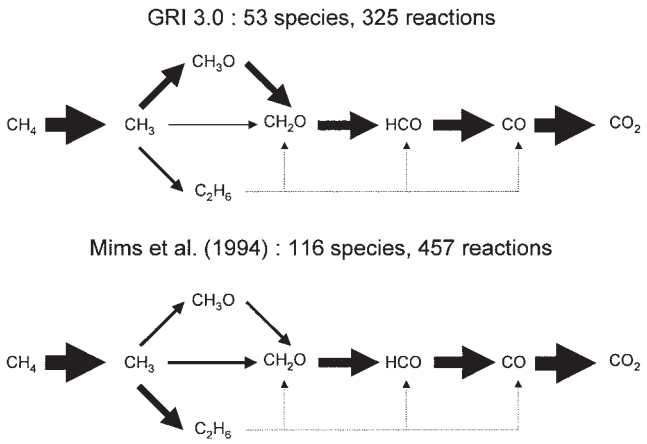

Figure 2. Time-integrated carbon element flux diagrams for mechanism comparison.

Adiabatic, PFR reactor simulation. Stoichiometric methane/air feed (methane:oxygen:nitrogen = 0.095/0.190/0.715); $P = 1$ atm. Diagrams compare two mechanisms and identify preferential decomposition pathways derived from time-integrated element flux analysis.

the calculation was performed at stoichiometric conditions and 1000 K (adiabatic), most hydrocarbons turn to CO and CO_2. The purpose of the exercise is not to compare the mechanisms and their respective validation, but rather to use those differences to exemplify the type of insight that can be so effectively generated by monitoring time-integrated elemental transformations.

Lean vs. Rich High-Temperature Methane Oxidation. An interesting analysis is to evaluate how the relative weights of the reaction pathways change as the reaction conditions change. An informative example for such an analysis is the comparison of the carbon element flux pathways under fuel-rich and fuel-lean conditions, as illustrated in Figure 3. Under fuel-rich conditions the pathways leading to C_2 chemistry are significantly more pronounced than those in the fuel-lean case, and the oxidation steps are more pronounced in the fuel-lean data set. This is further indication of the complication that arises in analysis and reduction of kinetic mechanisms. Different conditions (temperature, pressure, concentrations, etc.) activate significantly different chemistries.

Low-Temperature Hydrocarbon Oxidation. Although there are a number of large, detailed mechanisms for hydrocarbon oxidation, there is still significant improvement needed in these models. This is because many of the rate constants in the mechanisms are only estimated and some pathways (such as peroxy radical formation) are omitted to increase numerical efficiency. In addition to species reduction, the types of analysis described in this study can help identify the key reactions that need to be included or to have improved analysis of kinetic parameters (sensitivity).

Improved mechanisms for complex chemical processes in hydrocarbon oxidation are needed to implement advances in practical combustion devices. Of particular interest are the advanced internal combustion engines that will meet the strict environmental constraints of the future. The complexity of the phenomena is currently under intense investigation, both theoretically and experimentally (Griffiths, 1995). The accurate description of these processes requires detailed representation of the chemical kinetics, thus resulting in very large kinetic reaction schemes. A number of approaches have appeared in the literature that attempt to generate such schemes either manually (Curran et al., 1998b) or by computer-assisted automated procedures (Warth et al., 1998). Such reaction schemes offer an excellent test case for any automated computational analysis and reduction methodology. The intricacies of low-temperature oxidation of hydrocarbons have been extensively studied in a number of publications. The interested reader is referred to Tomlin et al. (1997) for a summary.

Figure 4 shows both the low- and high-temperature kinetic pathways for butane (C_4H_{10}, CCCC) oxidation. The secondary hydrogens (hydrogen atoms on CH_2 groups) have weaker bonds ($\sim$2.5 kcal mol^{-1}) than those of the primary hydrogen atoms. Thus at low temperature the secondary H's are lost first (by abstraction reaction) and a secondary butyl radical is formed (C·CCC). At low temperatures, oxygen adds to the butyl radical forming a butylperoxy radical (Figure 4)

$$\text{CC·CC} + \text{O}_2 \rightarrow \text{CC(OO·)CC} \tag{7}$$

The peroxy radical [CC(OO·)CC] isomerizes by hydrogen atom transfer to hydroperoxide–butyl radical [CC(OOH)CC·]

$$\text{CC(OO·)CC} \rightarrow \text{CC(OOH)CC·} \tag{8}$$

The hydroperoxide–alkyl radical reacts with a second oxygen, undergoes similar isomerization (hydrogen transfer) and decomposes through two different paths to lower energy, chain-branching products: (i) 2 OH radicals plus an aldehyde and (ii) a diradical + OH)

$$\text{CC(OOH)CC·} + \text{O}_2 \rightarrow \text{CC(OOH)CCOO·} \tag{9}$$

$$\text{CC(OOH)CCOO·} \rightarrow \text{CC·(OOH)CCOOH} \rightarrow \text{CC(=O)CCO·} + \text{·OH} + \text{·OH} \quad \text{(i)} \tag{10}$$

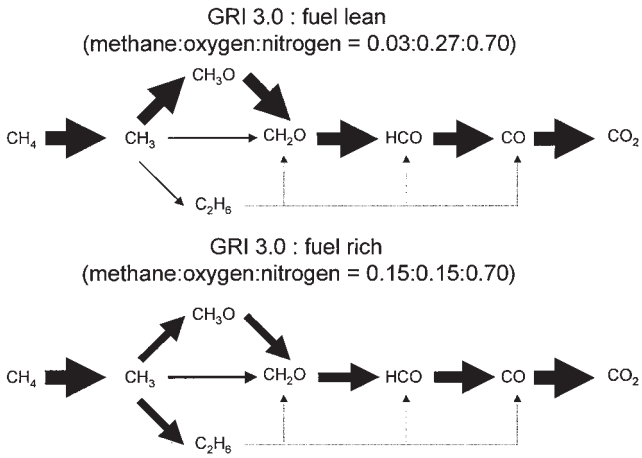

Figure 3. Fuel lean vs. fuel rich C element flux pathways.

Importance identified based on results on time integrated element flux analysis.

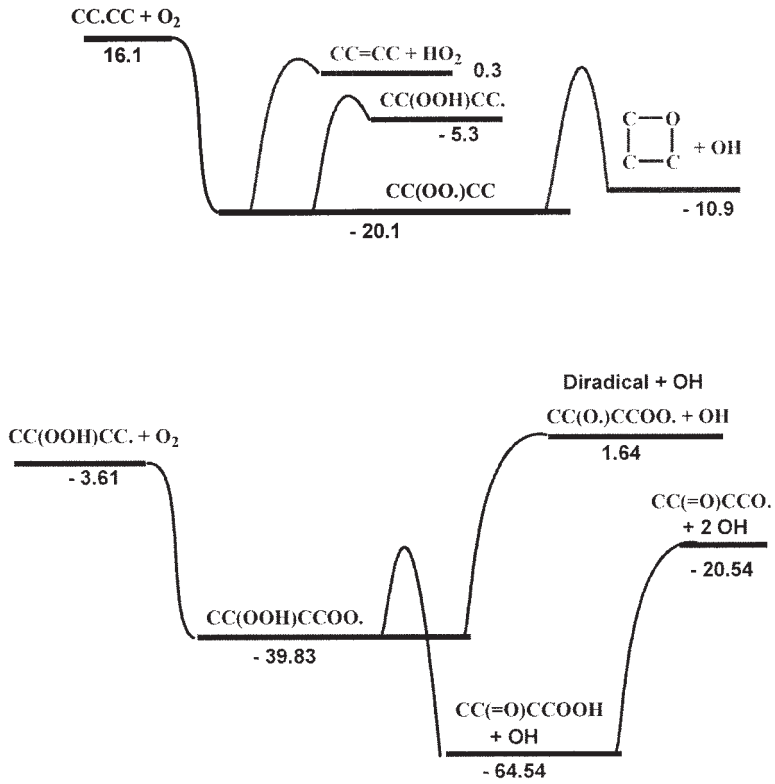

Figure 4. Potential energy diagram for chain-branching pathways that occur at moderate to low temperatures and lack of chain branching (chain propagation only) at somewhat higher (intermediate) temperatures.

At very high temperatures the secondary *n*-butyl radical will under go unimolecular reaction (beta scission) to form propene + methyl radical.

$$\searrow \text{CC(O}\cdot\text{)CCOO}\cdot + \cdot\text{OH} \qquad \text{(diradical + OH)} \qquad \text{(ii)} \tag{11}$$

These paths are chain branching and are responsible for an increase in oxidation rate that leads to the formation of cool flames.

As temperature increases the unimolecular dissociation reactions of the initial butyperoxy and the hydroperoxide–butyl radicals become more important and addition of the second oxygen becomes disfavored. In addition an alternate reaction path, HO_2 molecular elimination starts to become more important and this significantly limits the extent of chain branching. These can be described (Figure 4) as

$$\text{CC}\cdot\text{CC} + \text{O}_2 \leftarrow \text{CC(OO}\cdot\text{)CC} \qquad \text{(reverse, dissociation reaction)}$$

$$\text{CC(OOH)CCOO}\cdot \leftarrow \text{CC}\cdot\text{(OOH)CCOOH} \qquad \text{(reverse, dissociation reaction)}$$

$$\text{CCOO}\cdot\text{CC} \rightarrow \text{CC}{=}\text{CC} + \text{HO}_2 \qquad \text{(molecular elimination)}$$

$$\text{CC(OOH)CC}\cdot \rightarrow \text{Cyclic ether} + \text{OH} \qquad \text{C—cy(CCCO)} \tag{12}$$

Qualitatively, the resulting products from these two alternate paths amount to replacing the two active OH radicals by one OH or an even less reactive HO_2, which slows the oxidation process. This is the phenomenon known as *negative temperature coefficient* (NTC), where the apparent rate of oxidation decreases with increasing temperature attributed to reduced forward reaction. As the temperature of the system increases further, usually above 900–950 K, the pathway of the first oxygen addition becomes less favorable and β-scission (unimolecular dissociation processes of the hydrocarbon radical, not reaction with O_2) dominate

$$\text{CC}\cdot\text{CC} \rightarrow \text{CC}{=}\text{C} + \text{CH}_3\cdot \qquad \text{(beta scission)} \tag{13}$$

This defines the more usual high temperature oxidation chemistry of hydrocarbons (Wilk et al., 1995).

Recently, the combustion group at Lawrence Livermore National Laboratory published a detailed mechanism for hydrocarbon oxidation that includes much of the above-mentioned kinetics (chemical activation reactions and diradical product omitted; Curran et al., 1998a). A version of the mechanism containing 385 species and 1895 reactions was analyzed using the integrated element flux analysis approach. The conditions discussed in Minetti et al. (1996) were used for the analysis. Table 2 depicts the pathways that the time-integrated element flux analysis identifies as the critical ones, vs. initial

Table 2. Characteristic Hydrocarbon Oxidation Pathways*

				T = 1000 K				
OUTLET		C5H11-2	[49.93%]					
	###	C5H11-2	→	C3H6	→	C3H5-A	→	C3H5O
	→	C2H3CHO	→	C2H3CO	→	C2H3	→	C2H2
	→	HCCO	→	CO	→	CO2		
OUTLET		C5H11-1	[25.15%]					
	###	C5H11-1	→	NC3H7	→	C2H4	→	C2H3
	→	C2H2	→	HCCO	→	CO	→	CO2
OUTLET		C5H11-3	[24.93%]					
	###	C5H11-3	→	C4H8-1	→	C4H7	→	C4H7O
	→	C2H3CHO	→	C2H3CO	→	C2H3	→	C2H2
	→	HCCO	→	CO	→	CO2		
				T = 700 K				
OUTLET		C5H11-2	[49.74%]					
	###	C5H11-2	→	C5H11O2-2	→	C5H10OOH2-4	→	C5H10OOH2-4O2
	→	NC5KET24	→	CH3COCH2	→	CH3COCH2O2	→	CH3COCH2O2H
	→	CH3COCH2O	→	CH3CO	→	CO	→	CO2
OUTLET		C5H11-1	[25.43%]					
	###	C5H11-1	→	C5H11O2-1	→	C5H10OOH1-3	→	C5H10OOH1-3O2
	→	NC5KET13	→	C2H5CHO	→	C2H5CO	→	C2H5
	→	C2H5O	→	CH3CHO	→	CH3CO	→	CO
	→	CO2						
OUTLET		C5H11-3	[24.83%]					
	###	C5H11-3	→	C5H11O2-3	→	C5H10OOH3-2	→	C5H10-2
	→	C5H9	→	C3H6	→	C3H5-A	→	C3H5O
	→	C2H3CHO	→	C2H3CO	→	C2H3	→	C2H2
	→	HCCO	→	CO	→	CO2		
				T = 850 K				
OUTLET	###	C5H11-2	[49.92%]					
		C5H11-2	→	C3H6	→	C3H5-A	→	C3H5O
	→	C2H3CHO	→	C2H3CO	→	C2H3	→	C2H2
	→	HCCO	→	CO	→	CO2		
OUTLET		C5H11-1	[25.23%]					
	###	C5H11-1	→	C5H11O2-1	→	C5H10OOH1-3	→	C5H10O1-3
	→	C4H8-1	→	C4H7	→	C4H7O	→	C2H3CHO
	→	C2H3CO	→	C2H3	→	C2H2	→	HCCO
	→	CO	→	CO2				
OUTLET		C5H11-3	[24.84%]					
	###	C5H11-3	→	C5H11O2-3	→	C5H10OOH3-2	→	C5H10-2
	→	C5H9	→	C3H6	→	C3H5-A	→	C3H5O
	→	C2H3CHO	→	C2H3CO	→	C2H3	→	C2H2
	→	HCCO	→	CO	→	CO2		

*As an example, C5H11-1 represents the primary alkyl radical of pentane, C5H11-2 the secondary, etc. Each pathway represents the cascading of carbon element flux from the initial feed, through intermediates, with final products CO, CO2, plus other combustion products.

temperature of oxidation. At 1000 K β-scission of the hydrocarbon (*n*-butyl radical = C═C + CC–) dominates all the low-temperature pathways. At 700 K the O_2 addition reactions described above are important and at 850 K the unimolecular dissociation of the peroxy radical and the hydroperoxide–butyl radical are important. We can rationalize the key pathways present in this very detailed kinetic mechanism with minimal computational effort. This analysis will be important in trying to automate the coupling between mechanism generation and mechanism reduction in a unified framework.

The time-integrated pointers very efficiently generated the necessary information, which is required to begin rationalizing the key pathways present in a very detailed kinetic mechanism with minimal computational effort. The goal of the effort is to develop computational tools that enable the analysis of very large kinetic mechanisms generated using computer-assisted tools. In complicated and detailed mechanisms it becomes extremely difficult to trace the leading pathways simply by using intuition of analysis techniques that look at specific points in time. Furthermore, this analysis will be important in trying to automate the coupling between mechanism generation and mechanism reduction in a unified framework as will be presented later in this report.

Time-integrated element flux analysis in flames

In certain cases, explicit calculation of the quantities defined by Eq. 6a may not be feasible. Therefore, the analysis just presented has to be extended to account for situations where the required species and temperature profiles are the output of a "black-box" simulation and the generated information is then postprocessed.

To illustrate this approach we analyze the reaction pathways in a reaction–diffusion system such as a flame speed calculation. The SANDIA flame code is used to perform these calcu-

Table 3. Low- vs. High-Temperature Butane Pathways*

Low-temperature C4H10 oxidation—PFR simulation								
OUTLET		1 SC4H9	[65.16%]					
	###	SC4H9	→	SC4H9O2	→	C4H8OOH2-3	→	C4H8-2
	→	C4H7	→	C4H7O	→	C2H3CHO	→	C2H3CO
	→	C2H3	→	C2H2	→	HCCO	→	CO
	→	CO2						
OUTLET		2 PC4H9	[34.84%]					
	###	PC4H9	→	PC4H9O2	→	C4H8OOH1-3	→	C4H8OOH1-3O2
	→	NC4KET13	→	CH2CHO	→	C2H3O1,2	→	CH3CO
	→	CO	→	CO2				
High-temperature C4H10 oxidation—Freely propagating flame (SANDIA code)								
OUTLET		1 SC4H9	[66.94%]					
	###	SC4H9	→	C3H6	→	C3H5-A	→	C2H2
	→	HCCO	→	CO	→	CO2		
OUTLET		2 PC4H9	[32.43%]					
	###	PC4H9	→	C2H4	→	C2H3	→	C2H2
	→	HCCO	→	CO	→	CO2		
OUTLET		3 C2H5	[0.64%]					
	###	C2H5	→	C2H4	→	C2H3	→	C2H2
	→	HCCO	→	CO	→	CO2		

*PC4H9 denotes the primary butane decomposition radical C · *CCC*, *SC4H9 is the secondary radical*, *CC · CC. The carbon pathways denote the leading pathways indicating the cascading of the fuel* (*C4H10*) *down to combustion products such as CO*, *CO2*, *etc*.

lations (Kee et al., 1990). The flame calculations solve the following two-point boundary value problem

$$\dot{M} = \rho u A$$

$$\dot{M}\frac{dT}{dt} - \frac{1}{c_P}\frac{d}{dx}\left(\lambda A \frac{dT}{dx}\right) + \frac{A}{c_P}\sum_{k=1}^{K}\rho Y_k V_k c_{Pk}\frac{dT}{dx} + \frac{A}{c_P}\sum_{k=1}^{K}\dot{\omega}_k h_k W_k = 0$$

$$\dot{M}\frac{dY_k}{dt} + \frac{d}{dx}(\rho A Y_k V_k) - A\dot{\omega}_k W_k = 0 \qquad k = 1, \ldots, M$$

$$\rho = \frac{P\bar{W}}{RT} \tag{14}$$

Here, ρ denotes the density of the gas mixture, A is the area of the flame, c_P is the specific heat capacity, x is the axial coordinate, P is pressure, and $\dot{M}$ is the mass flow rate.

The analysis, based on discrete data, was used to derive element flux diagrams from flame speed simulations. The species profiles can also be used and postprocessed to generate the required information. The approach is illustrated for identifying the differences between high- and low-temperature oxidation. The mechanism discussed by Curran et al. (1998a) is used to perform flux analysis in an adiabatic plug-flow reactor with a stoichiometric mixture of butane and air starting at 700 K, and a flame calculation of a similar composition mixture, both at ambient conditions. Table 3 depicts the pathway differences when flux analysis is performed on flow reactor vs. flame conditions. The plug-flow reactor analysis is low-temperature oxidation and thus the associated pathways by peroxy radicals

Table 4. Cumulative Fractional OH Sources

Low T Oxidation			High T Oxidation		
FROM	TO	%	FROM	TO	%
HO2	OH	28.8	O2	OH	52.3
O2	OH	55.3	O	OH	81.0
H2O2	OH	72.2	HO2	OH	99.9
O	OH	85.5	C4H8OOH1-3	OH	99.9
CH3O2H	OH	88.0	C4H8OOH2-4	OH	100.0
C4H8OOH2-4O2	OH	90.4	CH3O2H	OH	100.0
NC4KET24	OH	92.8	C2H3CHO	OH	100.0
C4H8OOH1-3O2	OH	94.6	C4H8OOH2-4O2	OH	100.0
NC4KET13	OH	96.4	NC4KET24	OH	100.0
CH3COCH2O2H	OH	98.1	C4H8OOH1-3O2	OH	100.0
C4H8OOH1-3	OH	99.0	NC4KET13	OH	100.0
C4H8OOH2-4	OH	99.5	CH2CHO	OH	100.0
CH2CHO	OH	99.8	C4H8O1-3	OH	100.0
C2H3CHO	OH	100.0	CH3COCH2O2H	OH	100.0

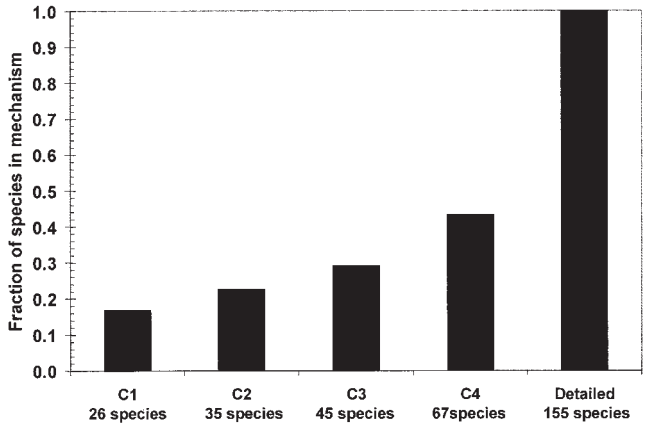

Figure 5. C_1–C_4 reduced mechanisms accounting for 85% element mass flux.

Analysis based on detailed mechanism of Marinov et al. (1998).

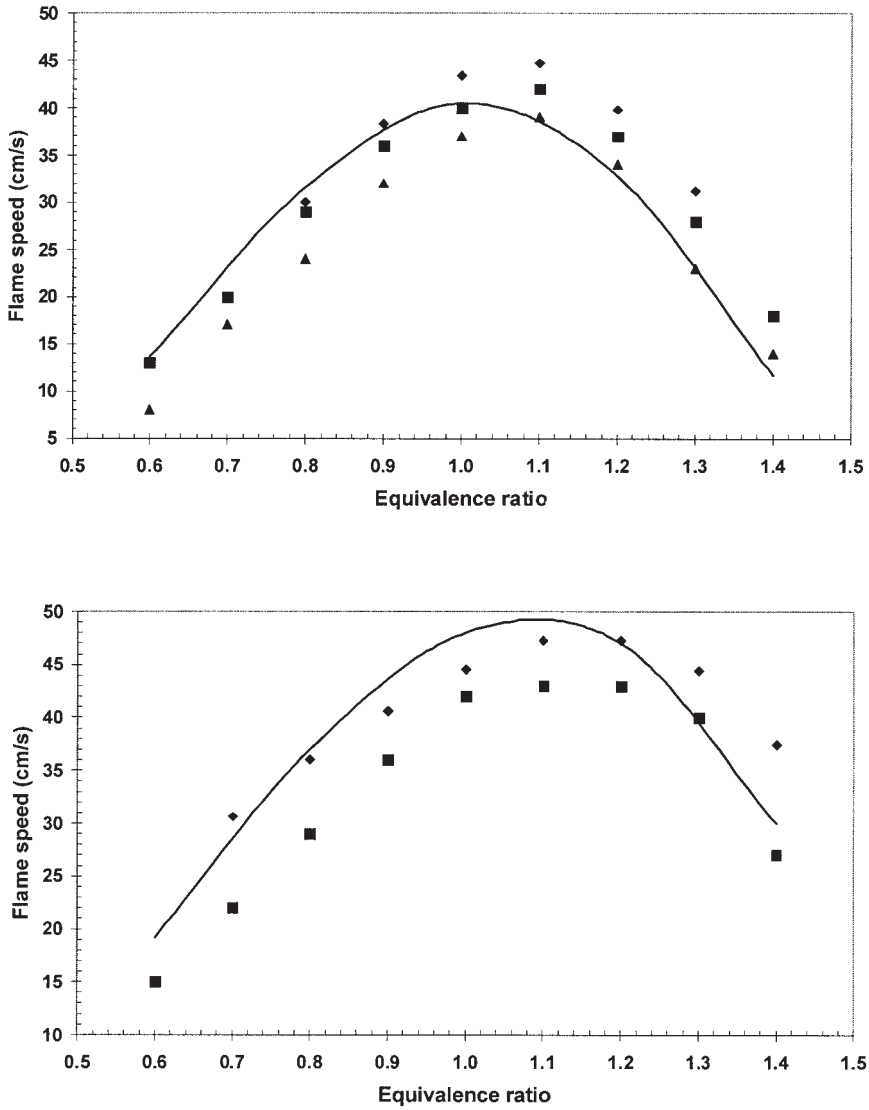

Figure 6. Stoichiometric methane–ethane flame speed at atmospheric conditions.

Solid symbols are experiments, solid line model predictions.

are the primary outlets for the fuel. The high-temperature chemistry, which is active during the stabilized flame operation, makes such pathways negligible.

One of the key characteristics of high- vs. low-temperature oxidation is that at low temperatures additional pathways become active that allow additional production of OH radicals. As seen from Table 4, at high temperatures the primary OH sources are H + O_2 and O + OH (that is, the standard routes), whereas at low temperatures about 15% of OH production is attributed to pathways active exclusively by the peroxy radical chemistry. The thermodynamic control of the kinetics gives rise to distinctly different pathways and, hence, very different chemical transformations in different temperature regimes. The important point is that the postprocessing of the flame data was able to correctly identify the different contributions of high- and low-temperature chemistry pathways.

Using time-integrated diagrams to identify skeletal reduced mechanisms

Flame Speed Predictions. The mechanism discussed in Marinov et al. (1998) was analyzed for the purpose of deriving subsets of the reactive species that would adequately predict C_1–C_4 flame speeds. The original mechanism contains 155 species and 689 reactions. Time-integrated flux analysis was performed at nominal conditions of stoichiometric mixtures at 1300 K. Because we are primarily interested in flame chemistry, focusing on high-temperature oxidation is a good indicator of the chemical phenomena occurring. Skeletal mechanisms of reduced size were identified (Figure 5) and the reduced mechanisms were subsequently used in conjunction with the SANDIA flame code to predict laminar flame speeds. The agreement of the reduced skeletal mechanism with experiments is excellent, as shown in Figures 6 and 7, for methane, ethane, propane, and butane.

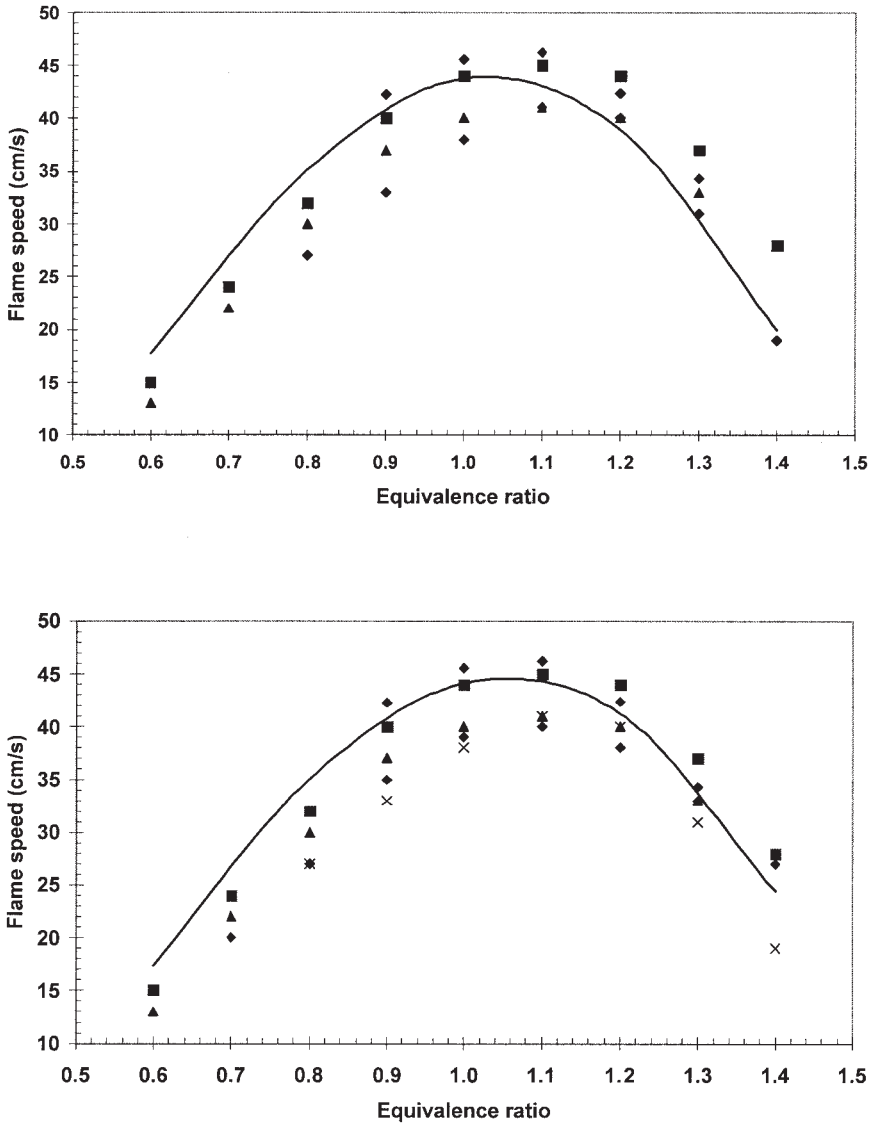

Figure 7. Stoichiometric propane–butane flame speed at atmospheric conditions.

Solid symbols are experiments; solid line, model predictions.

The concept of time-integrated element flux analysis is also used to identify the impact of molecular structure on fuel decomposition pathways in Farrell et al. (2004). They discuss an extensive experimental study examining the impact of molecular structures on flame speed measurements. The flux analysis is used to interpret the relationship between flame speed, molecular structure, and combustion chemistry.

Low-Temperature Autoignition Delays. The mechanism discussed in Curran et al. (1998b) was analyzed using the time-integrated element flux procedure to derive reduced mechanisms for low-temperature oxidation. In particular, we were interested in evaluating the ability of reduced mechanisms to predict low-temperature autoignition delays (Minnetti et al., 1996). Autoignition delay defines a fundamental property of fuels. It describes the time required for a mixture of fuel and air to autoignite at a given initial pressure and temperature. Experiments are conducted on a rapid compression machine (RCM). The mixture is quickly compressed to a target initial pressure and the corresponding temperature is calculated as the adiabatic compression temperature. In the calculation, the mixture is modeled using a constant volume combustion process at the initial conditions of the compressed mixture. The mixture is allowed to autoignite at these conditions and the time lag is recorded.

The mechanism of Curran et al. (1998) was used and size reduction performed. A number of skeletal mechanisms were developed according the desired % flux threshold. Autoignition delays were then predicting using significantly reduced mechanisms (75 species) and the detailed mechanism (385 species) and the predictions compared with experiments (Figure 8). The time-integrated element flux analysis procedure has resulted in a substantially reduced size model able to accurately capture the nonlinear behavior of the combustion systems and low temperatures.

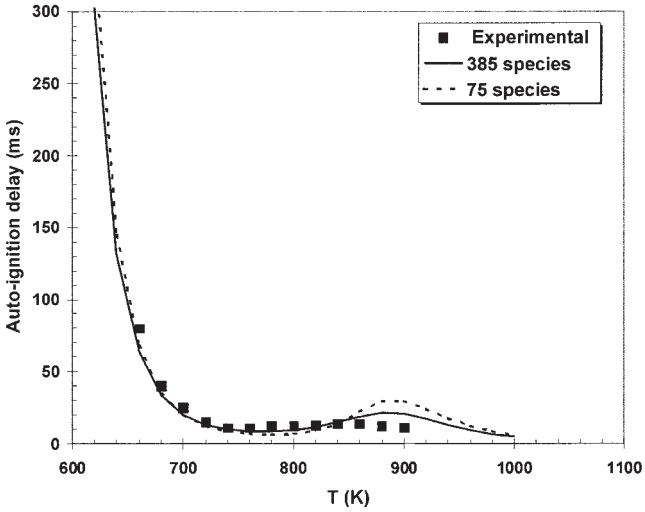

Figure 8. *n*-Pentane autoignition delay of stoichiometric–air mixtures for mean compressed charge density 135.5 mol m^{-3}.

Coupling Automated Generation and Integrated Element Flux Analysis

The algorithm and underlying computational approaches for automated construction of kinetic mechanisms were previously described (Grenda et al., 2002). This methodology automates the construction of detailed, elementary-step, chemical kinetic mechanisms using structural-based reaction algorithms. The approach includes newly developed algorithms to estimate required kinetic information of specific reaction classes, including more rigorous treatment of chemically activated reaction pathways. The mechanisms are constructed by using rules for determining permutations of possible products from reactants, identifying species structures, and generating required nomenclature, estimating the required reaction rates, and identifying the species and reactions that are kinetically significant (Grenda et al., 2001).

Overview of automated mechanism generation

The generation procedure begins using a set of initial (feed) species to initiate the reaction process by providing a set of reactants in a practical problem. The main algorithm is the reaction generator that lists all of the possible reactions of a given species. At a given point during the construction of the reaction scheme, some of the species are identified as "kinetically significant" and included in the mechanism, whereas others have been generated as products by reactions of the "significant" species, but have not been included as a possible reactant species. There are then two designations of species: those that appear only as products and those that appear as both reactants and products. As the algorithm progresses and reacts, species to generate chemical reactions become available. The process is continual and iterative: species whose production rates are initially determined to be insignificant are continually being reevaluated to assess whether they have evolved to be significant. The process is described in Figure 9 and is explained in greater detail in the aforementioned references.

The incorporation of flux analysis in this automated mechanism generation is a significant improvement over previous work. The element-based analysis allows the current status of the mechanism to be reevaluated as the mechanism is *developing*, rather than the traditional approach of waiting until a complete mechanism has been generated before analysis and reduction are started.

The approach is used to address two important problems in automated mechanism generation. First, the mechanism generation process is a computationally intensive procedure where all of the possible reaction pathways are explored regardless of their kinetic impact on the mechanism. The complexity is increased when chemically activated reaction paths are added in the mechanism generation process. Second, the number of species generated during the mechanism building process is very large.

The current approach represents a significant advancement in that the relative importance of all the species in the mechanism is reevaluated at any desired point. The mechanism is complete when the species M with the largest production rate is less than a certain value (Susnow et al., 1997). The externally defined rate criterion is defined as R_{min} = (precision level) × R_{char}. Clearly, as the precision tightens, the number of species with formation rates large enough that they must be included in the mechanism increases. The mechanism generator iterates at a particular conversion level until no unreacted species have

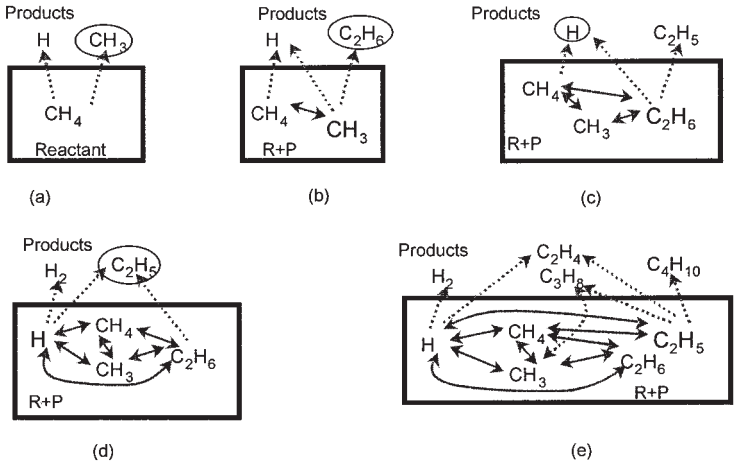

Figure 9. Schematic of the mechanism generation algorithm using the validation case of methane pyrolysis.

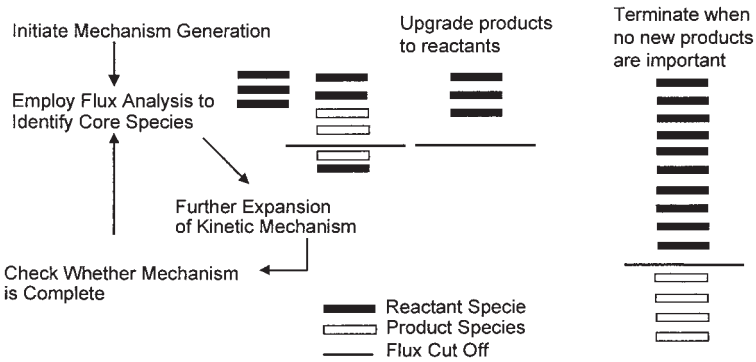

Figure 10. Computational framework for combining element flux analysis and automated mechanism generation.

formation rates greater than the R_{min}. The flux analysis is performed relative to externally specified cutoff criteria E_{min}, denoting the percentage flux, per element, that is retained in the mechanism. The flux analysis is a time-integrated procedure and is performed in line with the mechanism generation iteration.

Here it is important to specify cutoff parameters, which are not so restrictive as to discard the underlying physical processes for both the mechanism generation and reduction procedures. This is most simply tested by performing analyses to several levels of precision until the predictive results do not change significantly. Our ongoing area of work is focused on more rigorously investigating the role and sensitivity of the approach to species generation and flux tolerance levels. The process is described in Figure 10. The time-integrated element flux analysis is used to assess the impact of species created during the generation process and to determine whether they should be included and participate as reactants in future steps.

Computer-generated mechanism for methane pyrolysis

The formation of ethane in methane pyrolysis is a strongly nonlinear process and serves as a validation example to demonstrate the capability of the numerical mechanism generation algorithm. The operating conditions at 1058 K isothermal and 0.58 atm were selected to be consistent with available experimental data (Back and Back, 1983).

Validation of the Reduction Process. A number of mechanisms were generated using different values of the termination criterion to generate mechanisms of different size. For each mechanism, the time-integrated element flux analysis identified skeletal, reduced schemes, which are illustrated in Table 5. These results show that beyond a certain size of the detailed mechanism (31 species), the reduced models are converging. This is an indication that the basic chemistry in the mechanism generator library of reactions has been captured. Any additional increase of the detailed mechanism does not introduce any new features to the chemistry. The successful combination of automated mechanism generation and reduction should therefore automatically create a mechanism with the appropriate size.

Comparison of the different mechanism predictions indicates that the reduction process properly identifies the critical required size of the reduced mechanisms. These results are depicted in Figure 11. The solid lines show the numerical predictions for different product species as a function of time, and the solid symbols represent available experimental data. The significant time delay after which the production of ethane begins to accelerate nonlinearly can be readily seen in the experimental data. Previous work (Dean, 1990) has demonstrated that the experimental results can be explained by a series of chemically activated pathways involving the C_5 radical species. These results include the numerical predictions for the mechanism generation process without the coupled mechanism reduction process. The RN7 curve indicates the numerical prediction of ethane concentration as a function of time for the mechanism generation process at a relatively tight precision of 0.0001. The number of species in this mechanism is 82 among a set of 1138 reactions. The agreement with the experimental data is seen to be quite good, and captures the details of the ethane acceleration. An identical prediction using a flux cutoff precision of 0.1 is given by the RN1 curve. For this much less restrictive condition, the generated mechanism is much smaller, containing only 20 species and 102 reactions and does not reproduce the reaction data. Further details can be found in Grenda et al. (2001).

A number of computational experiments, coupling automated mechanism generation and reduction, are depicted in Figure 12. The combined approach converges to the ideal mechanism as the generation method becomes more accurate and the flux criterion for species retention more strict.

Table 5. Generated and Reduced Mechanisms for Methane Pyrolysis

Automated Generated Mechanisms				Reduced Mechanisms, 95% mass flux		
Mechanism	Accuracy	# Species	# Reactions	Mechanism	# Species	# Reactions
RN1	1.E-01	20	102	RN1-reduced	13	62
RN2	1.E-02	34	207	RN2-reduced	21	105
RN3	1.E-03	46	426	RN3-reduced	27	197
RN4	1.E-04	56	567	RN4-reduced	31	271
RN7	1.E-07	82	1138	RN7-reduced	31	271

Furthermore, at no time during the generation process does the size of the mechanism become prohibitively large. Although, as indicated in Table 5, the mechanism can reach 82 species and over 1000 reactions during the generation process, the combination of generation/reduction never generates more than 30 species and 270 reactions. The advantage of this combined approach is that instead of generating detailed mechanisms that will then have to be reduced, we generate a smaller-size mechanism from the very beginning.

For this calculation the frequency of reduction is held constant and only the element flux cutoff is varied to estimate the impact on the generation process. The following are some key observations:

(1) The procedure after a small number of iterations converges to a consistent scheme beyond which further increase of the detailed mechanism has no impact. For example, the 99.5% carbon mass flux cutoff identifies a critical reduced mechanism of 27 species. Further application of the generation rules results in mechanisms that, upon reduction, produce the same 27-species mechanism.

(2) The expected size of the mechanism grows as we allow for higher carbon flux.

(3) No mechanism is generated that is as large as RN7 that was generated above. One of the main advantages, and driving force behind such a combined scheme, is to prevent the generation process from creating overly detailed mechanisms. We attempt to identify the critical chemical information and make sure that, at any time, only this is maintained and further refined on-line.

It is the focus of our current research to optimize a number of computational parameters involved in such a scheme. These include (a) the frequency of reduction and (b) on-line estimation of flux cutoff criteria based on the predictive response of the generated mechanism (either by comparisons between detailed and reduced model data or by comparisons with available data).

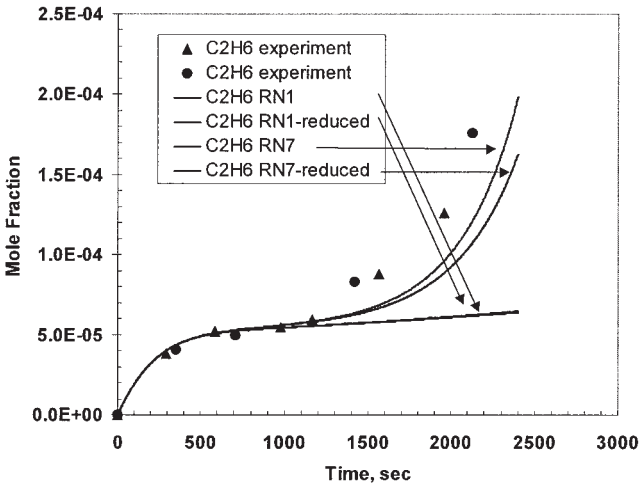

Figure 11. Comparison of experimental and numerical predictions for the production of ethane as a function of time for methane pyrolysis.

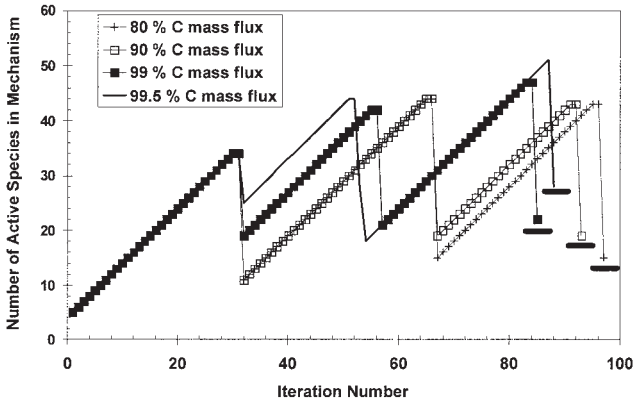

Figure 12. Combined application of automated mechanism generation and on-line reduction based on time-integrated element flux.

Caveat

There is always the possibility that a mechanism being analyzed and/or undergoing the process of reduction, may be missing important reactions. Alternately the mechanism generator may not include a class of reaction or a type of species. The kinetic effects resulting from omitted reactions or species cannot be incorporated into the reduced mechanism or model, and the mechanism may be inaccurate under some application conditions. Improvements in the reaction kinetics and paths are ongoing as well as improvements in thermochemistry and thermochemical property estimation techniques. The analysis, sensitivity, and size reduction of the mechanism will, however, be facilitated with the techniques in this study.

Concluding Remarks

This study revisited the concept of element flux analysis and demonstrates a method to derive time-independent quantities to define global element flux summary. The flux results can then be used for the analysis and reduction of complex kinetic mechanisms. Three novel aspects in the computational analysis of complex kinetic mechanisms are illustrated:

(1) The introduction of a time-integrated analysis provides a global view of the transformations during the reaction interval.

(2) Unlike other analysis techniques, the approach is readily applicable to complicated reactive flow systems and the principles are demonstrated by analyzing flame code outputs.

(3) A novel coupling of automated mechanism generation and reduction is presented that greatly enhances the efficiency of computer generated kinetic mechanisms as it allows for the on-the-fly analysis and reduction of the generated mechanism, thus maintaining a manageable size of the final mechanism.

The approach is illustrated by analyzing a highly detailed mechanism of low temperature oxidation of pentane and flame speed prediction of a variety of hydrocarbons. Excellent agreement between detailed original models and highly reduced kinetic models are obtained over a wide range of operating conditions. Finally, it is shown how incorporating the concept of time-integrated element flux significantly enhances automated mechanism generation procedures through a fully coupled generation/reduction procedure. Ongoing work is directed at additional systems relevant to hydrocarbon combustion.

Literature Cited

Back, M. H., and R. A. Back, "Thermal Decomposition and Reactions of Methane," *Pyrolysis: Theory and Industrial Practice*, L. F. Albright, B. L. Crynes, and W. H. Concoran, eds., Academic Press, New York (1983).

Broadbelt, L. J., S. M. Stark, and M. T. Klein, "Computer-Generated Pyrolysis Modeling: On the Fly Generation of Species, Reactions and Rates," *Ind. Eng. Chem. Res.*, **33**, 790 (1994).

Chevalier, C., W. J. Pitz, J. Warnatz, C. K. Westbrook, H. Melenk, "Hydrocarbon Ignition: Automatic Generation of Reaction Mechanisms and Applications to Modeling of Engine Shock," *Proc. Combust. Inst.*, **24**, 1362 (1992).

Curran, H. J., P. Gaffuri, W. J. Pitz, and C. K. Westbrook, "A Comprehensive Modeling Study of *n*-Heptane Oxidation," *Combust. Flame*, **114**, 149 (1998b).

Curran, H. J., W. J. Pitz, C. K. Westbrook, C. V. Callahan, and F. L. Dryer, "Oxidation of Automotive Primary Reference Fuels at Elevated Pressures," Proc. of the 27th Int. Symp. on Combustion, The Combustion Institute, Pittsburgh, PA, pp. 379–387 (1998a).

Dean, A. M. "Detailed Kinetic Modeling of Autocatalysis in Methane Pyrolysis," *J. Phys. Chem.*, **94**, 32 (1990).

Farrell, J. T., R. J. Johnston, and I. P. Androulakis, "Molecular Structure Effects on Laminar Burning Velocities at Elevated Temperature and SAE paper 2004-01-2936 (2004).

Grenda, J. M., I. P. Androulakis, and J. W. Bozzelli, "Combined Use of Automated Kinetic Mechanism Generation and Reduction in the Development of Chemical Reaction Models," 2nd Joint Meeting of the U.S. Sections of the Combustion Institute, Oakland, CA (2001).

Grenda, J. M., I. P. Androulakis, A. M. Dean, and W. H. Green, "Application of Computational Kinetic Mechanism Generation to Model the Autocatalytic Pyrolysis of Methane," *Ind. Eng. Chem. Res.*, **42**(5), 1000 (2002).

Kee, R. J., F. M. Rupley, E. Meeks, and J. A. Miller, "Chemkin—III: A Fortran Chemical Kinetics Package for the Analysis of Gas-Phase Chemical and Plasma Kinetics," SANDIA Report, SAND96-8216 (1996).

Marinov N. M., W. J. Pitz, C. K. Westbrook, A. M. Vincitore, M. J. Castaldi, and S. M. Senkan, "Aromatic and Polycyclic Aromatic Hydrocarbon Formation in a Laminar Premixed *n*-Butane Flame," C*ombust. Flame*, **114**, 192 (1998).

Mims, C. A., R. Mauti, A. M. Dean, and K. D. Rose, "Radical Chemistry of Methane Oxidative Coupling: Tracing of Ethylene Secondary Reactions with Computer Models and Isotopes," *J. Phys. Chem.*, **98**, 13357 (1994).

Revel, J., J. C. Boettner, M. Cathonet, and J. S. Bachman, "Derivation of a Global Kinetic Mechanism for Methane Ignition and Combustion," *J. Chim. Phys. Phys.-Chim. Biol.*, **91**, 365 (1994).

Smith, G. P., D. M. Golden, M. Frenklach, N. W. Moriarty, B. Eiteneer, M. Goldenberg, C. T. Bowman, R. K. Hanson, S. Song, W. C. Gardiner, V. V. Lissianski, and Z. Qin, GRIMECH 3.0, http://www.me.berkeley.edu/gri_mech/

Susnow, R. G., A. M. Dean, W. H. Green, P. Peczak, and L. J. Broadblet, "Rate-Based Construction of Kinetic Models for Complex Systems," *J. Phys. Chem.*, **101**, 3731 (1997).

Tomlin, A. S., T. Turányi, and M. J. Pilling, "Mathematical Tools for the Construction, Investigation and Reduction of Combustion Mechanisms," *Low-Temperature Combustion and Autoignition*, Elsevier, Amsterdam (1997).

Turányi, T., and T. Berges, "Reaction Rate Analysis of Complex Kinetic Mechanisms," *Int. J. Chem. Kinet.*, **21**, 83 (1989)

Warth, V., F. Battin-Leclerc, R. Fournet, P. A. Glaude, G. M. Come, and G. Scacchi, "Computer-Based Generation of Reaction Mechanisms for Gas-Phase Oxidation," *Comput. Chem.*, **24**, 541 (2000).

Westbrook, C. K., "The Internal Combustion Engine at Work," http://www.llnl.gov/str/Westbrook.html (2002).

Wilk, R. D., R. S. Cohen, and N. P. Cernasky, "Oxidation of n-butane-Transition in the Mechanism Across the Region of Negative Temperature Coefficient," *Ind. Eng. Chem. Res.,* **34**(7), 2285 (1995).

Manuscript received Aug. 25, 2003, and revision received Feb. 26, 2004.